Hindawi
Advances in High Energy Physics
Volume 2017, Article ID 6708581, 10 pages
https://doi.org/10.1155/2017/6708581

Research Article

A New Two-Component Model for Hadron Production in Heavy-Ion Collisions

Xuejiao Yin,[1] LiLin Zhu,[1] and Hua Zheng[2]

[1]*College of Physical Science and Technology, Sichuan University, Chengdu 610064, China*
[2]*Laboratori Nazionali del Sud, INFN, Via Santa Sofia 62, 95123 Catania, Italy*

Correspondence should be addressed to Hua Zheng; zheng@lns.infn.it

Received 16 February 2017; Accepted 19 April 2017; Published 23 May 2017

Academic Editor: Ming Liu

Using the experimental data from the ALICE program on the centrality dependence of the transverse momentum (p_T) spectra in Pb+Pb collisions at $\sqrt{s_{\mathrm{NN}}} = 2.76$ TeV, we show that the double-Tsallis distribution and the generalized Fokker-Planck (FP) solution cannot describe the spectra of pions, kaons, and protons from central to peripheral collisions in the entire p_T region, simultaneously. Hence, a new two-component distribution, which is a hydrodynamic extension of the generalized FP solution accounting for the collective motion effect in heavy-ion collisions, is proposed in order to reproduce all the identified particle spectra. Our results suggest that the particle production dynamics may be different for different particles, especially at very low p_T region.

1. Introduction

The advent of a new generation of high energy colliders, such as Relativistic Heavy-Ion Collider (RHIC) and Large Hadron Collider (LHC), has launched a new era in the study of the hadron production. Plenty of pp, pA, and AA collisions data have been accumulated, which allow one to study the nature of the final particle production. The particle transverse momentum spectra carry important information about the dynamics of particle production and evolution process of interacting system formed in high energy nuclear collisions. In the past decade, the attempt to understand the particle production mechanism by different theoretical and phenomenological approaches has been a great success [1–22]. Generally, the theoretical investigation of hadron production in heavy-ion collisions is operated into different camps, characterized by the regions of transverse momenta p_T of the produced hadrons. At low p_T statistical hadronization and hydrodynamical models are generally adopted [1–3], whereas at high p_T jet production and parton fragmentation with suitable consideration of medium effects in perturbative QCD (pQCD) are the central themes [4–6]. The approaches have been studied essentially independent of each other with credible success in interpreting the experimental data for different p_T regions, since their dynamics are decoupled.

At intermediate and lower p_T recombination or coalescence subprocess (ReCo) in heavy-ion collisions has been found to be more relevant, which has successfully explained various experimental data [7–9]. Beside the ReCo model, there are also other phenomenological models proposed to describe the hadron production. In [10, 11], within the two-component model, treating the particle spectra as a summation of an exponential (Boltzmann-like) and power-law distributions was suggested. However this model could not describe the charged particle production at very high p_T in central Pb+Pb collisions at 2.76 TeV. So an additional power-law term was added, which was explained by the peculiar shape of the nuclear modification factor R_{AA}. On the other hand, due to the effect of the collective motion in large colliding system, the relativistic hydrodynamics are usually adopted to consider the particle production, instead of thermodynamic methods. Therefore, the charged particle

spectra could be consisting of a hydrodynamic term and two power-law terms suggested as well in [10],

$$\frac{\mathrm{d}N}{p_T \mathrm{d}p_T} = A_e \int_0^R r\,\mathrm{d}r m_T I_0\left(\frac{p_T \sinh\rho}{T_e}\right) K_1\left(\frac{m_T \cosh\rho}{T_e}\right) + \frac{A}{\left(1 + p_T^2/\left(T^2 \cdot N\right)\right)^N} + \frac{A_1}{\left(1 + p_T^2/\left(T_1^2 \cdot N_1\right)\right)^{N_1}}, \quad (1)$$

where $\rho = \tanh^{-1}\beta_r$ is the transverse flow rapidity and the radial flow velocity is parametrized as $\beta_r(r) = \beta_s r/R$ with $\beta_s = 0.5c$ for the surface velocity. R is a parameter related to the transverse size of the particle distribution in space and r is the distance of the particle from the origin of the coordinate system in the transverse plane. $m_T = \sqrt{m^2 + p_T^2}$ is the transverse mass and m is the rest mass of particle. I_0 and K_1 are the modified Bessel functions. Hence, there are eight free parameters A_e, T_e, A, T, N, A_1, T_1, and N_1, which add the difficulty to fit, although (1) can describe the charged particle spectra very well in central Pb+Pb collisions. Other forms of multicomponent models, which were derived from multisource thermal model [12–14], were also applied to the particle transverse momentum spectra produced from low energy to high energy heavy-ion collisions.

Besides, the Tsallis distribution, which was proposed about three decades ago [23], has been widely applied to describe final particle production with great success by the theorists and experimentalists [15–22]. It was derived in the framework of nonextensive thermodynamics,

$$f(E,q) = A\left[1 + (q-1)\frac{E-\mu}{T}\right]^{-(1/(q-1))}, \quad (2)$$

where q is the entropic factor, which measures the nonadditivity of the entropy, and T is the temperature. The two parameters carry important information of the observed colliding system. E is the energy of the particle. μ is the chemical potential which could be assumed to be 0, when the colliding energy is high enough, and the chemical potential is much smaller than the temperature. If the self-consistent thermodynamical description is taken into account, the effective distribution $[f(E,q)]^q$ is needed [16, 17, 19]. One should bear in mind that even though different versions of Tsallis distribution were adopted by different groups in the literature, it has established the excellent ability to describe the hadron spectra in a large p_T region in pp, pA, and AA collisions. Here we will try to pursue this approach to the identified particles in the noncentral Pb+Pb collisions at $\sqrt{s_{\mathrm{NN}}} = 2.76$ TeV. Furthermore, for comparison, we will also discuss the particle spectra in the frame of Fokker-Planck equation and try to get some information about the hadron production during the evolution of the colliding system.

The paper is organized as follows. In Sections 2 and 3, we show our results of particle spectra from Pb+Pb collisions with a double-Tsallis distribution as well as the generalized Fokker-Planck solution, respectively. A new two-component distribution which is consisting of the hydrodynamic term and generalized Fokker-Planck solution is proposed in Section 4. In Section 5, a detailed comparison among the three distributions is shown. Finally, a summary is given in Section 6.

2. A Double-Tsallis Distribution

In our earlier work [21], it has been demonstrated that a single Tsallis distribution could not fully reproduce the whole structure of the observed particle spectra in central Pb+Pb collisions at $\sqrt{s_{\mathrm{NN}}} = 2.76$ TeV. Therefore, a double-Tsallis distribution could be proposed,

$$\frac{\mathrm{d}N}{p_T \mathrm{d}p_T} = C_1 \cdot \left(1 + \frac{E_T}{m_1 T_1}\right)^{-m_1} + C_2 \cdot \left(1 + \frac{E_T}{m_2 T_2}\right)^{-m_2}, \quad (3)$$

where $E_T = \sqrt{m^2 + p_T^2} - m$ is the transverse energy. When the rest mass of particle $m \to 0$, (3) becomes the same as the double-Tsallis distribution proposed in [16] for charged particles, which are dominated by pions. But when m is large, such as kaons, protons, and antiprotons, the mass effect should be taken into account. The double-Tsallis distribution (3) is assumed by hadron yields stemming from two parts: soft and hard yields. Due to jet-medium interactions, it is almost impossible to distinguish the origin of the final particles. Thus, the yields from minijets are included in either the soft or hard contribution. Comparing with the single Tsallis distribution, three more parameters are increased, which allow one to fit the charged particle spectra with p_T up to 100 GeV/c in the most central Pb+Pb collisions [16]. Recently, the transverse momentum spectra of charged pions, kaons, and protons up to $p_T = 20$ GeV/c have been measured in Pb+Pb collisions at $\sqrt{s_{\mathrm{NN}}} = 2.76$ TeV using the ALICE detector for six different centrality classes [24]. Hence, it is the right time to investigate whether the double-Tsallis distribution can describe the identified particle production at both central and noncentral collisions.

As shown in Figure 1, (3) reproduces the data for pions and kaons very well, while for protons the situation is different. Firstly, it is remarkable that the spectrum of protons at the centrality 60–80% could be described by (3) very well, in agreement with the conclusion in our previous work [20]. The peripheral collisions in AA are more similar to the p+p collisions and the single Tsallis distribution can fit all the particle spectra produced [20]. Secondly, one could also notice that, in Figure 1(c) when $p_T \leq 2$ GeV/c, the lines are much larger than the data for central and less central collisions. The existence of difference is not surprising. Compared with pions and kaons, the spectra of protons demonstrate different behaviors at low p_T. This could be because the particle production dynamics are different for different particles. On the one hand, a cascade particle production mechanism was proposed in p+p collisions. The heavier particles are more likely to be produced at the beginning while the light particles can be produced at all times [20]. On the other hand, in the

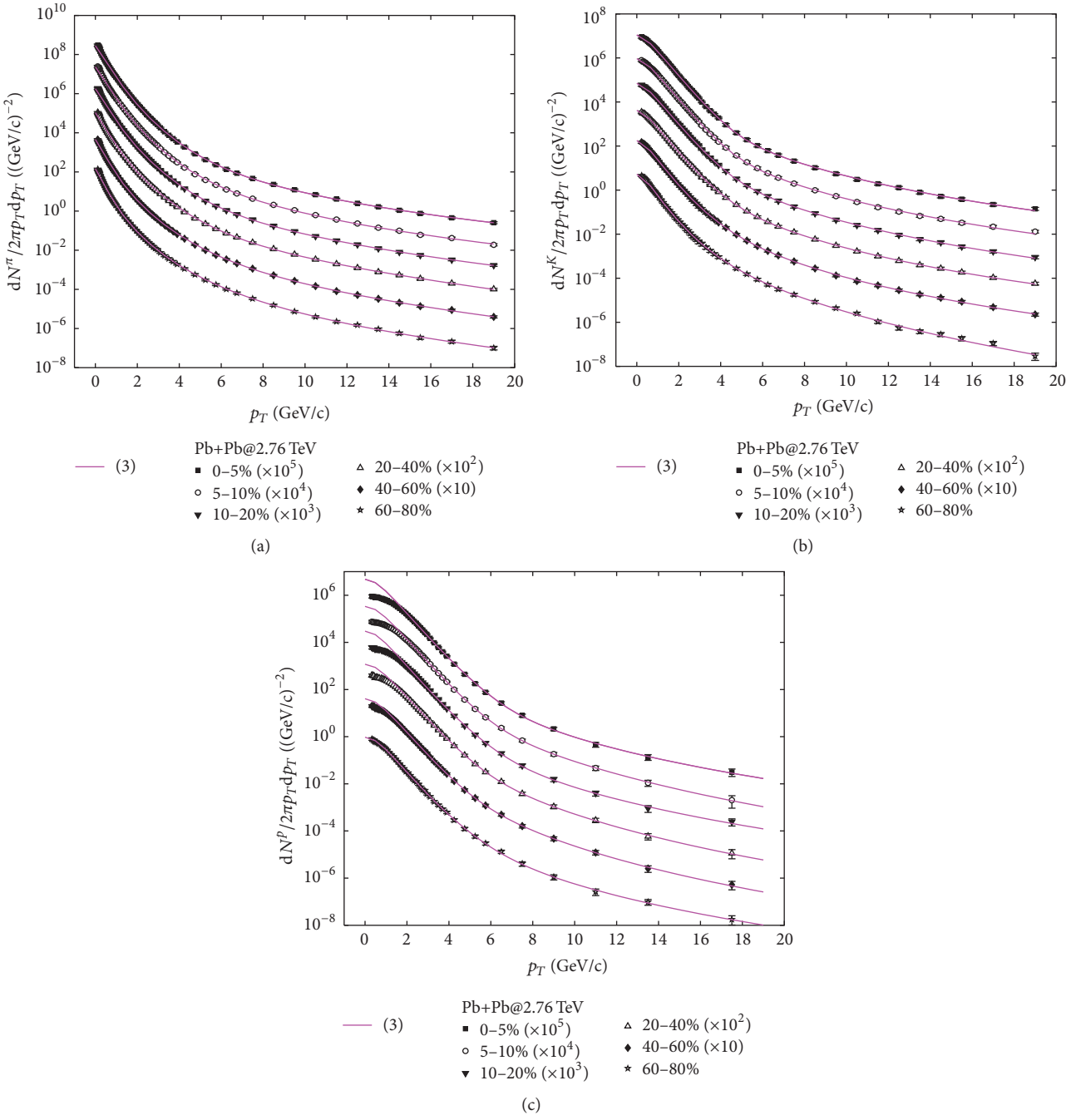

Figure 1: Fitting results using the double-Tsallis distribution (3) for (a) $\pi^+ + \pi^-$, (b) $K^+ + K^-$, and (c) $p + \overline{p}$ in Pb+Pb collisions at $\sqrt{s_{\mathrm{NN}}} = 2.76$ TeV. For a better visualization both the data and the analytical curves have been scaled by a constant as indicated. Data are taken from ALICE [24].

quark recombination models [7–9], mesons are formed by combining a quark and an antiquark while baryons by three quarks. Because different numbers of (anti)quarks participate in forming the particles, the structures of their spectra must be different. In this sense, our investigation results urge more studies on particle production mechanisms.

The fitting parameters can be found in Table 1. One can see that the two Tsallis distributions in (3) account for different p_T regions of the particle transverse momentum spectrum. The first one dominates in the low p_T region and is close to the exponential form, resulting in large value of m_1, while the second one is responsible for high p_T tail. Generally speaking, the temperature-like parameter T_1 can represent the temperature of the particles and it decreases from central to peripheral collision for pions, kaons, and protons. One should bear in mind that the discrepancy observed on the fit

Table 1: The fitting parameters for various particles with double-Tsallis distribution (3).

Particle	Centrality [%]	C_1	T_1	m_1	C_2	T_2	m_2
$\pi^+ + \pi^-$	0–5	2811.28	0.200	12.55	13.47	0.251	5.92
	5–10	2322.40	0.199	12.28	13.74	0.256	6.12
	10–20	1805.78	0.194	11.16	0.219	0.656	7.47
	20–40	1079.34	0.182	9.79	0.0134	1.222	10.66
	40–60	464.42	0.166	8.66	0.00530	1.137	9.59
	60–80	148.16	0.149	7.76	0.000958	1.040	8.18
$K^+ + K^-$	0–5	103.77	0.360	80.59	7.36	0.251	6.08
	5–10	84.95	0.359	71.49	8.68	0.242	6.13
	10–20	64.16	0.352	52.86	6.87	0.258	6.36
	20–40	36.89	0.332	31.41	5.00	0.254	6.36
	40–60	13.96	0.300	20.74	3.94	0.230	6.36
	60–80	5.26	0.251	11.71	0.0205	0.652	9.79
$p + \overline{p}$	0–5	45.64	0.364	34.50	2.04	0.253	6.61
	5–10	33.40	0.378	43.49	0.375	0.412	8.12
	10–20	29.41	0.351	27.33	0.435	0.334	6.92
	20–40	10.86	0.385	47.70	0.991	0.309	7.75
	40–60	3.47	0.377	45.53	0.604	0.290	7.67
	60–80	0.915	0.341	21.39	0.0359	0.325	6.79

for protons at low p_T (see Figure 1(c)) definitely affects the T_1 value. T_1 for kaons is a little bit smaller than the one for protons at the same centrality and both are larger than that of pions. This observation is similar to the case in p+p collisions [20, 22].

3. The Generalized Fokker-Planck Solution

The Fokker-Planck equation has a wide amount of applications in different fields. For instance, FP equation has been solved to study the time evolution of income distributions for different classes in a country [25], the rapidity spectra for net proton production at RHIC, SPS, and AGS [26], and the interaction of nonequilibrated heavy quarks with the quark-gluon plasma expected to be formed in heavy-ion collisions at RHIC and LHC energies [27–30]. The general form of Fokker-Planck equation is [27]

$$\frac{\partial P(r,t)}{\partial t} = \frac{\partial}{\partial r}\left[A(r)P(r,t)\right] + \frac{\partial^2}{\partial r^2}\left[B(r)P(r,t)\right]. \quad (4)$$

The coefficients $A(r)$ and $B(r)$ are the drift and diffusion terms, respectively. Here, t represents the time while r is the variable studied, which we have chosen as E_T, based on the same consideration as in (3). Assuming $A(E_T) = A_0 + \alpha E_T$ and $B(E_T) = B_0 + \beta E_T^2$, one could obtain the stationary solution $P_s(E_T)$ of (4)

$$P_s(E_T) = A\frac{e^{-(b/T)\arctan(E_T/b)}}{\left[1+(E_T/b)^2\right]^c}, \quad (5)$$

which fulfills the condition $\partial_t P_s = 0$ and depends on the three parameters $b = \sqrt{B_0/\beta}$, $T = B_0/A_0$, and $c = 1 + \alpha/2\beta$. When $p_T \ll 1$ or $(E_T/b) \ll 1$, from (5), we can get

$$P_s(E_T) \propto e^{-(E_T/T)}. \quad (6)$$

On the other hand, when $p_T \gg 1$ or $E_T/b \gg 1$, (5) becomes

$$P_s(E_T) \propto p_T^{-2c}. \quad (7)$$

The asymptotic behaviors of $P_s(E_T)$ are consistent with those of transverse momentum distribution of the final particles in heavy-ion collisions, which exhibits roughly a power-law distribution for large p_T, whereas it becomes purely exponential for small p_T. Actually, in [21], we have proposed a formula for the first time, which is similar to (5), to fit all the particle spectra at central collisions in Pb+Pb at $\sqrt{s_{\mathrm{NN}}} = 2.76$ TeV but the power of E_T/b in the denominator of (5) was fixed and changed from 2 to 4. We realize that we need to generalize the formula proposed in [21] in order to describe the spectra of identified particles at both central and noncentral collisions. The generalized form of the solution of Fokker-Planck equation is

$$\frac{\mathrm{d}N}{p_T \mathrm{d}p_T} = A\frac{e^{-(b/T)\arctan(E_T/b)}}{\left[1+(E_T/b)^d\right]^c}. \quad (8)$$

There are five parameters A, b, c, d, and kinetic temperature T. This distribution interpolates between the exponential law for low p_T and the power-law for high p_T. A crossover between the two regimes takes place at $E_T \sim b$. In Figure 2, we redo the fitting with (8). The corresponding parameters are listed in Table 2. One can see that the power d for pions, kaons, and protons is close to 4 at central collisions, in agreement with our previous work [21] where $d = 4$ is fixed. We also find that d decreases from central to peripheral collisions for all the particles. As we have mentioned above, d is equal to 2 in the stationary solution of FP equation. Therefore, it could be interesting to explore the time evolution of this power by solving the FP equation to look for more insights. But this is

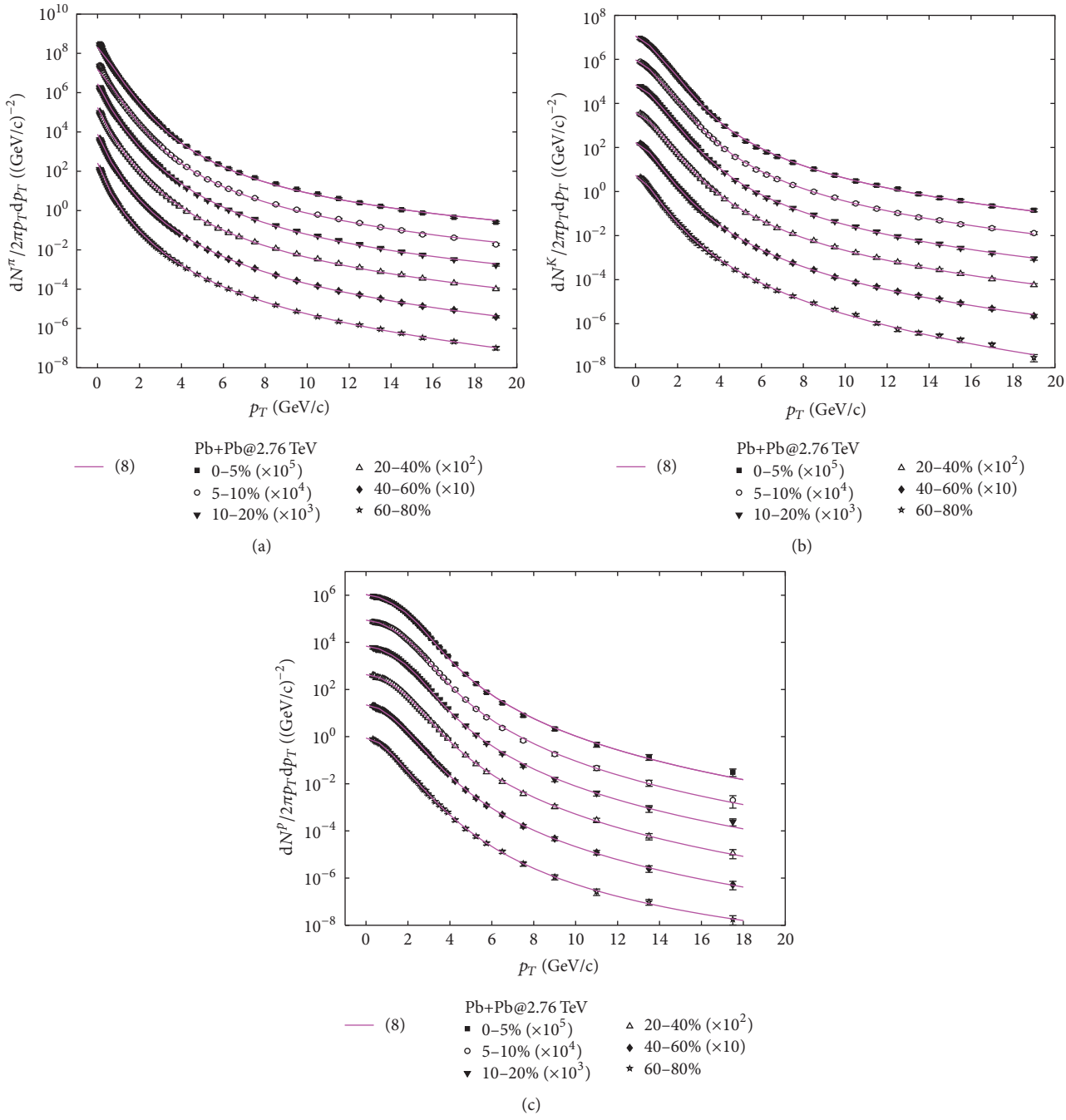

FIGURE 2: Fitting results using the generalized Fokker-Planck solution (8) for (a) $\pi^+ + \pi^-$, (b) $K^+ + K^-$, and (c) $p + \overline{p}$ in Pb+Pb collisions at $\sqrt{s_{NN}} = 2.76$ TeV. For a better visualization both the data and the analytical curves have been scaled by a constant as indicated. Data are taken from ALICE [24].

out of the scope of this paper. Since the exponent of power-law term in the denominator of (8) is the product of c and d when $p_T \gg 1$, this means they are coupled. Actually, Table 2 shows that c and d have opposite behaviors versus centrality for pions, kaons, and protons. The parameter T for pions and kaons increases while it decreases for protons with the centrality. The results show us that we cannot interpret the parameter T as the temperature of the final particles and it must be correlated with the other fitting parameters.

In Figure 2, we can see that the fits are better than the ones with (3), especially for protons. But for pions, the solid lines are a little bit lower than the data at $p_T < 1$ GeV/c for central collisions. In log scale the difference is invisible. We will show this in linear scale at Section 5. This leads us to figure out another method to illustrate the spectra of pions at very low p_T region. At the same time, it also should be able to reproduce kaons and protons production. In other words, we hope that there is a universal distribution, which

Table 2: The fitting parameters for various particles with the generalized FP solution (8).

Particle	Centrality [%]	A	T	b	c	d
$\pi^+ + \pi^-$	0–5	2040.75	0.2533	2.195	0.923	3.862
	5–10	1533.20	0.2726	2.122	1.536	2.647
	10–20	2844.93	0.4382	3.820	6.934	0.632
	20–40	1737.89	0.4906	3.750	7.942	0.638
	40–60	769.90	0.5887	3.526	9.384	0.654
	60–80	262.31	0.7224	3.320	10.765	0.653
$K^+ + K^-$	0–5	114.94	0.3344	1.802	0.921	4.833
	5–10	95.24	0.3375	1.842	0.974	4.523
	10–20	69.00	0.3545	1.890	1.274	3.533
	20–40	38.19	0.3686	2.079	1.670	2.651
	40–60	16.63	0.5205	3.069	4.635	1.088
	60–80	5.488	0.9863	2.444	7.186	0.981
$p + \overline{p}$	0–5	10.62	0.6943	1.849	1.543	4.134
	5–10	8.82	0.7038	1.849	1.650	3.867
	10–20	6.95	0.6816	1.839	1.636	3.813
	20–40	4.29	0.6731	1.839	1.936	3.189
	40–60	2.23	0.5207	2.023	2.036	2.798
	60–80	0.871	0.4465	4.254	2.712	1.260

Table 3: The fitting parameters for pions with the hydrodynamic extension of the generalized FP solution (9).

Particle	Centrality [%]	A_e	T_e	A	T	b	c	d
$\pi^+ + \pi^-$	0–5	225795.0	0.0798	1318.27	0.2804	2.019	1.245	3.398
	5–10	151041.0	0.0886	891.47	0.3017	1.901	1.472	3.125
	10–20	124015.0	0.0864	657.78	0.3095	1.932	1.628	2.837
	20–40	73316.2	0.0886	295.77	0.3455	1.805	1.972	2.523
	40–60	36461.8	0.0853	94.49	0.4247	1.593	2.647	2.084
	60–80	13825.1	0.0797	25.75	0.5582	1.414	3.444	1.737

could describe the spectra of the different final particles for the whole p_T region.

4. A New Two-Component Distribution

Recognizing that both the double-Tsallis distribution and the generalized Fokker-Planck solution are not able to fully reproduce the observed structure at low p_T region, it is argued that one should realize that the soft and hard particles have different production mechanisms. We need to figure out how to make the fit for pions better at very low p_T since (8) can fit kaons and protons very well; see Figures 2(b) and 2(c). The bulk of low-p_T particles originates from the "quark-gluon soup" formed in the heavy-ion collision and has an exponential distribution, while the high-p_T tail accounts for the minijets that pass through the hot medium, a process which can be described in pQCD. When a large colliding system is formed, one should also take the effects of the "collective motion" into account [31]. Thus, in heavy-ion collisions multiparticle production is usually considered in terms of relativistic hydrodynamics, contrary to the widely used thermodynamic approaches for pp, γp, and $\gamma\gamma$ collisions [23]. Therefore, we introduce a hydrodynamic extension to the generalized Fokker-Planck solution (8) to improve the fit for pions in Figure 2(a).

As shown in Figure 3(a), we present an example of the use of this method for pions at six different centralities in Pb+Pb collisions using the following formula:

$$\frac{\mathrm{d}N}{p_T \mathrm{d}p_T} = A_e \int_0^R r\,\mathrm{d}r m_T I_0\left(\frac{p_T \sinh\rho}{T_e}\right) K_1\left(\frac{m_T \cosh\rho}{T_e}\right) + A\frac{e^{-(b/T)\arctan(E_T/b)}}{\left[1+\left(E_T/b\right)^d\right]^c}. \quad (9)$$

The results are indeed encouraging, even though two more parameters, A_e and T_e, are added. As shown in Table 3, T_e from the hydrodynamic term at all centralities are below the phase transition temperature $T_c \sim$ 155–160 MeV for QGP. This could be explained by considering that the expanding system cools down until it reaches the freeze-out stage. The

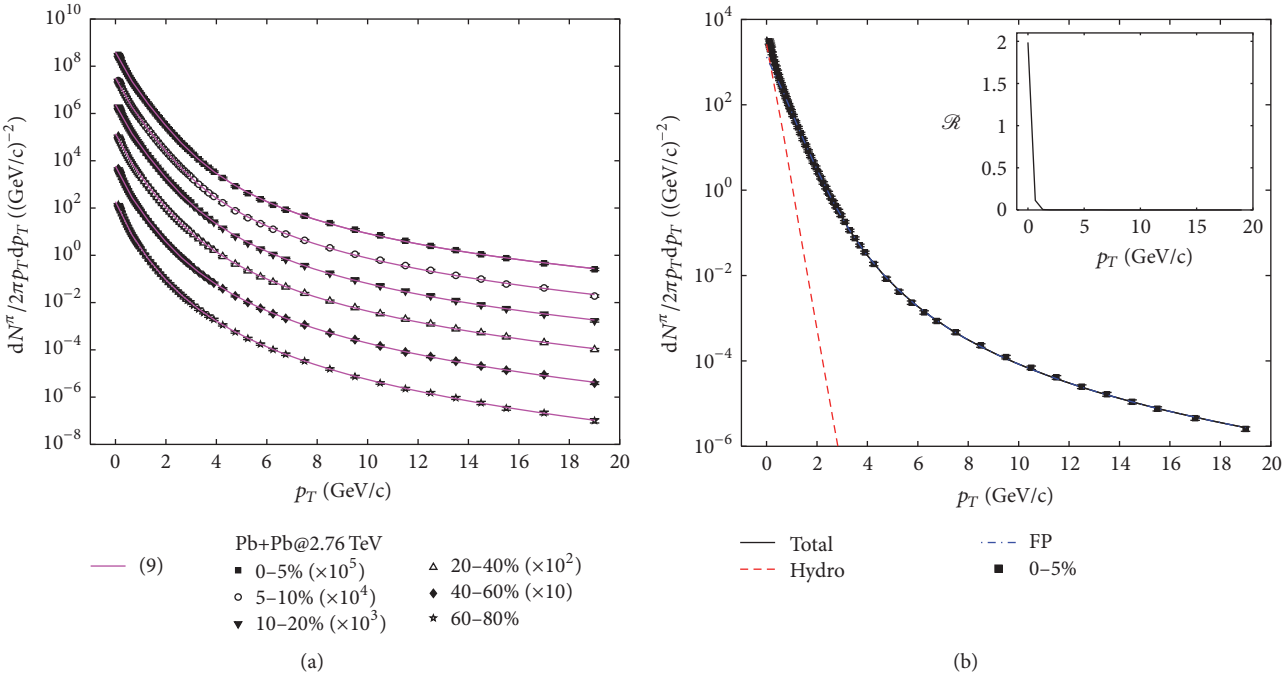

FIGURE 3: Fitting results using the new two-component distribution (9) for (a) $\pi^+ + \pi^-$, while in (b) the red (dashed) and blue (dash-dotted) lines show the hydrodynamic term (hydro) and the generalized Fokker-Planck term (FP) at centrality 0–5%, respectively. The inset is for the ratio of the two terms; see the context. Data are taken from ALICE [24].

parameters from the generalized FP solution have the same behavior as the ones in Table 2 and they are correlated as well. The solid lines include the total contributions from the hydrodynamic and generalized Fokker-Planck terms in (9). To get a clear picture of the two terms, we show them in different color lines for 0–5% in Figure 3(b). To show the difference clearly a ratio $\mathscr{R}$ of the hydrodynamic term over the generalized Fokker-Planck term is plotted in the inset of Figure 3(b) as a function of p_T. It indicates that the generalized Fokker-Planck term is absolutely dominant at $p_T > 1$ GeV/c, while the contribution from the hydrodynamic term definitely cannot be ignored at very low p_T region. When the contribution from hydrodynamic term is extremely small, (9) is the same as (8) and it can reproduce the particle spectra for kaons and protons. The results are similar to Figures 2(b) and 2(c) and we do not need to repeat them.

5. Discussion

Generally speaking, the results shown in the previous sections indicate that the three different methods, which are the double-Tsallis distribution (3), the generalized Fokker-Planck solution (8), and the new two-component distribution (9), can describe the experimental data. But we want to understand which distribution is the optimal choice. To have a clearer picture, we evaluate the degree of agreement of the fitted results with the experimental data. One can calculate the ratio between the experimental data and the fitted results, which is defined as

$$R = \frac{(\text{data} - \text{fitted})}{\text{data}}. \tag{10}$$

Figure 4 shows the ratio R, calculated by (3), (8), and (9), respectively, as a function of the transverse momentum p_T in linear scale for the centrality 0–5%. In Figure 4(a), one can see that all points for pions produced in most central collisions from (9) are in the range from −0.1 to 0.1, while the relative discrepancies from (3) and (8) are large at low p_T region. For kaons, (3) and (8) have the similar fitting power as shown in Figure 4(b), and the deviation of the fitting results from data is less than 10%, while, for protons, Figure 4(c) establishes that (3) is not good for low p_T region, which can be easily seen from Figure 1(c).

For the sake of the comprehensive comparison, we should also check the relative discrepancies of the three equations at other centralities. Here, we only plot the results for the centrality 60–80%, which are shown in Figure 5. Except for few points, the relative discrepancies of the three equations for pions, kaons, and protons are in good agreement with the data exhibiting deviations lower than 10%. Remarkably, the fluctuations for pions, kaons, and protons are much smaller than those for the centrality 0–5%. In other words, the three distributions nicely agree in describing the particle spectra produced in peripheral collisions, which are similar to p+p collisions.

Based on these analyses, we can conclude that (9), which is composed of a hydrodynamic term and the generalized Fokker-Planck solution, is the best one among the three distributions and it could well describe the spectra from central to peripheral collisions for pions, kaons, and protons. The proposed hydrodynamic extension (9) of (8) slightly modifies the description of the experimental data for pions

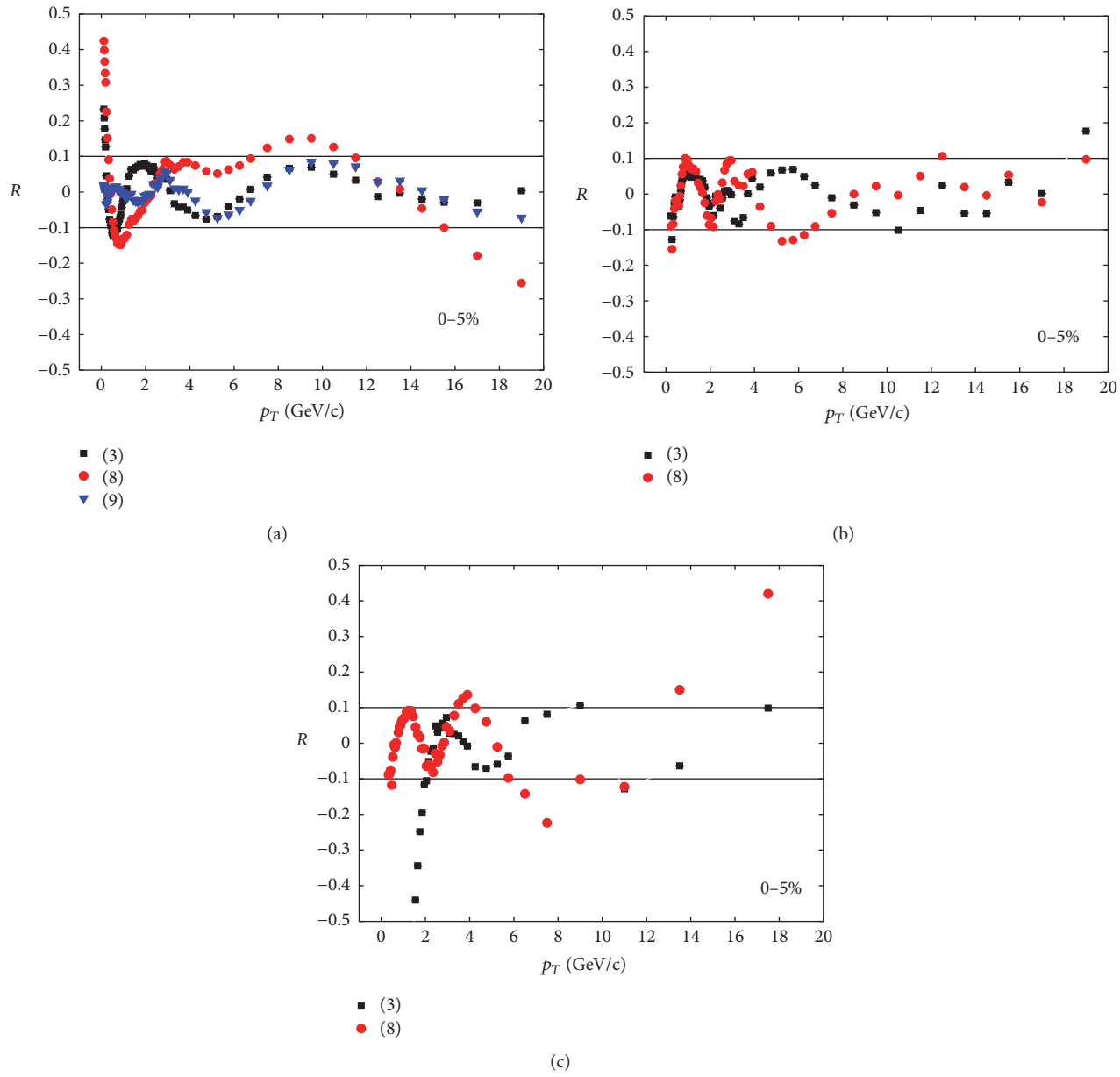

FIGURE 4: The relative discrepancies of (3), (8), and (9) from the p_T spectra for (a) $\pi^+ + \pi^-$, (b) $K^+ + K^-$, and (c) $p + \overline{p}$ at centrality 0–5% shown in Figures 1, 2, and 3, respectively.

at low p_T region, which also gives insight to the particle production mechanism.

6. Summary

In this paper, we have made a detailed study of the double-Tsallis distribution, the generalized Fokker-Planck solution, and the new two-component distribution, by fitting the transverse momentum spectra of pions, kaons, and protons in Pb+Pb collisions at $\sqrt{s_{\mathrm{NN}}} = 2.76$ TeV. The double-Tsallis distribution can fit the particle spectra except the big deviation observed for proton at $p_T < 2$ GeV/c for central and less central collisions, while the generalized Fokker-Planck solution is not able to describe the spectra of pions at very low p_T. Therefore, we propose a new two-component distribution as a hydrodynamic extension of the generalized Fokker-Planck solution accounting for the collective motion effect in order to fit all the particle spectra in Pb+Pb collisions, especially for extremely low p_T region. According to these results, we can conclude that the new two-component distribution is the optimal method. From these analyses, we get more information about the particle production mechanism in Pb+Pb collision. We also wish more exciting results could be found in Pb+Pb collisions at $\sqrt{s_{\mathrm{NN}}} = 5.02$ TeV.

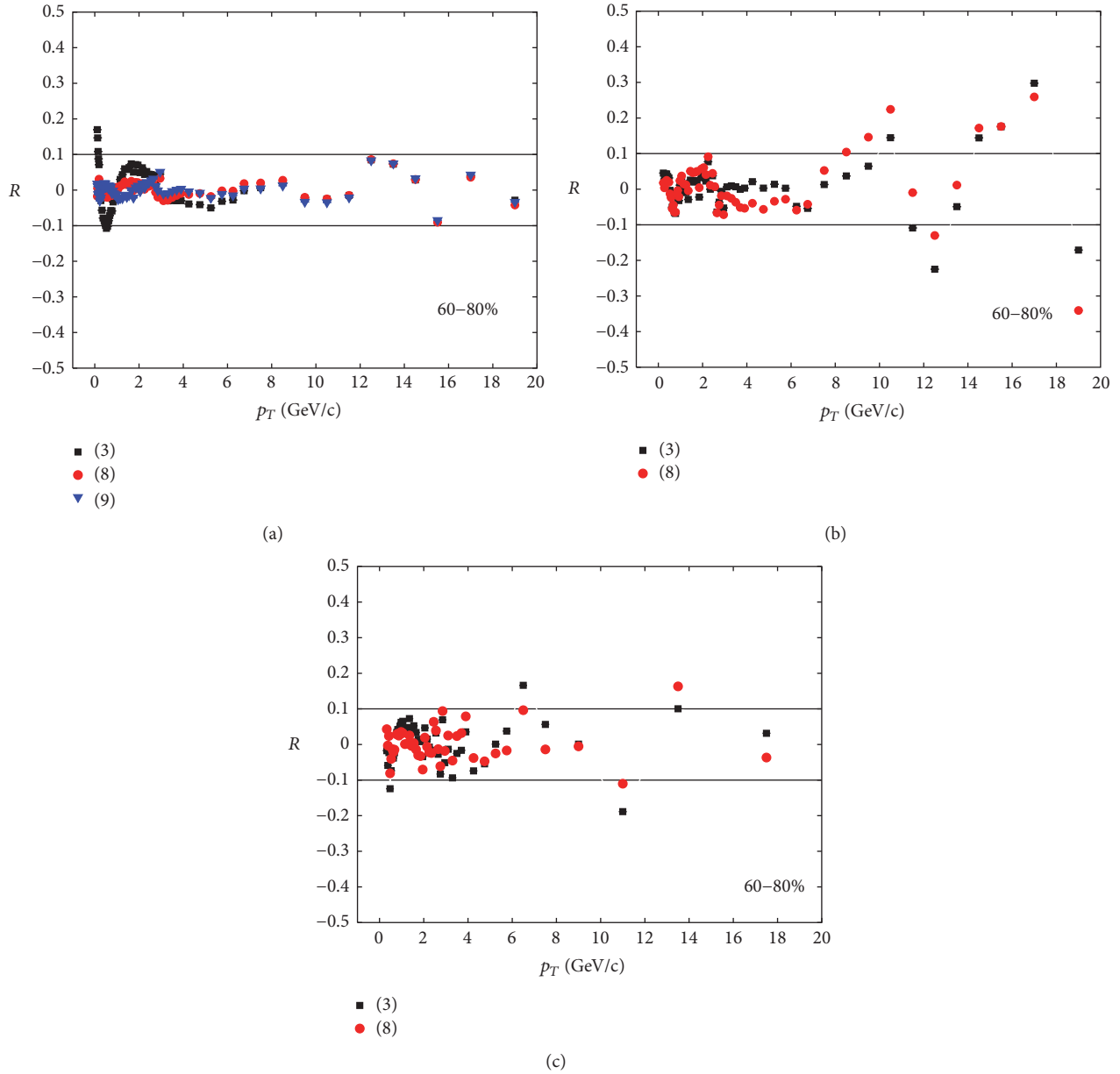

FIGURE 5: The relative discrepancies of (3), (8), and (9) from the p_T spectra for (a) $\pi^+ + \pi^-$, (b) $K^+ + K^-$, and (c) $p + \overline{p}$ at centrality 60–80% shown in Figures 1, 2, and 3, respectively.

Conflicts of Interest

The authors declare that there are no conflicts of interest regarding the publication of this article.

Acknowledgments

The authors thank Dr. S. Burrello for reading carefully their paper. This work is supported by the NSFC of China under Grant no. 11205106.

References

[1] P. Braun-Munzinger, K. Redlich, and J. Stachel, "Particle production in heavy ion collisions," in *Quark–Gluon Plasma 3*, R. C. Hwa and X.-N. Wang, Eds., p. 491, World Scientific, Singapore, 2004.

[2] P. F. Kolb and U. Heinz, "Hydrodynamic description of ultrarelativistic heavy ion collisions," in *Quark-Gluon Plasma 3*, R. C. Hwa and X.-N. Wang, Eds., p. 634, World Scientific, Singapore, 2004.

[3] C. Gale, S. Jeon, and B. Schenke, "Hydrodynamic modeling of heavy-ion collisions," *International Journal of Modern Physics A*, vol. 28, no. 11, Article ID 1340011, 2013.

[4] R. Baier, Y. L. Dokshitzer, A. H. Mueller, S. Peigne, and D. Schiff, "Radiative energy loss and $p_\perp$ broadening of high-energy partons in nuclei," *Nuclear Physics B*, vol. 484, pp. 265–282, 1997.

[5] X. Guo and X.-N. Wang, "Multiple scattering, parton energy loss, and modified fragmentation functions in deeply inelastic

eA scattering," *Physical Review Letters*, vol. 85, no. 17, pp. 3591–3594, 2000.

[6] K. M. Burke, A. Buzzatti, N. Chang et al., "Extracting the jet transport coefficient from jet quenching in high-energy heavy-ion collisions," *Physical Review C*, vol. 90, Article ID 014909, 2014.

[7] V. Greco, C. M. Ko, and P. Lévai, "Parton coalescence and the antiproton/pion anomaly at RHIC," *Physical Review Letters*, vol. 90, no. 20, Article ID 202302, 2003.

[8] R. J. Fries, B. Müller, C. Nonaka, and S. A. Bass, "Hadronization in heavy-ion collisions: recombination and fragmentation of partons," *Physical Review Letters*, vol. 90, no. 20, Article ID 202303, 2003.

[9] R. C. Hwa and C. B. Yang, "Recombination of shower partons at high p_T in heavy ion collisions," *Physical Review C*, vol. 70, Article ID 024905, 2004.

[10] A. A. Bylinkin, N. S. Chernyavskaya, and A. A. Rostovtsev, "Hydrodynamic extension of a two-component model for hadroproduction in heavy-ion collisions," *Physical Review C—Nuclear Physics*, vol. 90, no. 1, Article ID 018201, 2014.

[11] A. A. Bylinkin, N. S. Chernyavskaya, and A. . Rostovtsev, "Two components in charged particle production in heavy-ion collisions," *Nuclear Physics. B.*, vol. 903, pp. 204–210, 2016.

[12] H.-R. Wei, Y.-H. Chen, L.-N. Gao, and F.-H. Liu, "Comparing multicomponent Erlang distribution and Lévy distribution of particle transverse momentums," *Advances in High Energy Physics*, vol. 2014, Article ID 782631, 16 pages, 2014.

[13] F.-H. Liu, "Unified description of multiplicity distributions of final-state particles produced in collisions at high energies," *Nuclear Physics A*, vol. 810, no. 1–4, pp. 159–172, 2008.

[14] F.-H. Liu and J.-S. Li, "Isotopic production cross section of fragments in Fe-65 + p and Xe-136 (Xe-124) + Pb reactions over an energy range from A-300 to A-1500 MeV," *Physical Review C—Nuclear Physics*, vol. 78, no. 4, Article ID 044602, 2008.

[15] C. Wong and G. Wilk, "Tsallis fits to p_T spectra and multiple hard scattering in pp collisions at the LHC," *Physical Review D*, vol. 87, no. 11, Article ID 114007, 19 pages, 2013.

[16] M. Rybczyn'ski, G. Wilk, and Z. Włodarczyk, "System size dependence of the log-periodic oscillations of transverse momentum spectra," *EPJ Web of Conferences*, vol. 90, Article ID 01002, 6 pages, 2015.

[17] J. Cleymans and D. Worku, "The tsallis distribution in proton-proton collisions at $\sqrt{s}$ = 0.9 TeV at the LHC," *Journal of Physics G: Nuclear and Particle Physics*, vol. 39, no. 2, Article ID 025006, 2012.

[18] K. Aamodt, N. Abel, U. Abeysekara et al., "Production of pions, kaons and protons in pp collisions at $\sqrt{s}$ = 900 GeV with ALICE at the LHC," *The European Physical Journal C*, vol. 71, article 1655, 2011.

[19] F.-H. Liu, Y.-Q. Gao, and B.-C. Li, "Comparing two-Boltzmann distribution and Tsallis statistics of particle transverse momentums in collisions at LHC energies," *The European Physical Journal A*, vol. 50, article 123, 11 pages, 2014.

[20] H. Zheng, L. Zhu, and A. Bonasera, "Systematic analysis of hadron spectra in p+p collisions using Tsallis distributions," *Physical Review D*, vol. 92, Article ID 074009, 7 pages, 2015.

[21] H. Zheng and L. Zhu, "Can tsallis distribution fit all the particle spectra produced at RHIC and LHC?" *Advances in High Energy Physics*, vol. 2015, Article ID 180491, 9 pages, 2015.

[22] G. Bíró, G. G. Barnaföldi, T. S. Biró, K. Ürmössy, and Á. Takács, "Systematic analysis of the non-extensive statistical approach in high energy particle collisions—experiment vs. theory," *Entropy*, vol. 19, no. 3, Article ID 88, 21 pages, 2017.

[23] C. Tsallis, "Possible generalization of Boltzmann-Gibbs statistics," *Journal of Statistical Physics*, vol. 52, no. 1-2, pp. 479–487, 1988.

[24] J. Adam, D. Adamovà, M. M. Aggarwal et al., "Centrality dependence of the nuclear modification factor of charged pions, kaons, and protons in Pb-Pb collisions at $\sqrt{s_{NN}}$ = 2.76 TeV," *Physical Review C*, vol. 93, no. 3, Article ID 034913, 2016.

[25] A. Banerjee and V. M. Yakovenko, "Universal patterns of inequality," *New Journal of Physics*, vol. 12, Article ID 075032, 25 pages, 2010.

[26] W. M. Alberico and A. Lavagno, "Non-extensive statistical effects in high-energy collisions," *The European Physical Journal A*, vol. 40, no. 3, pp. 313–323, 2009.

[27] B. Svetitsky, "Diffusion of charmed quarks in the quark-gluon plasma," *Physical Review D*, vol. 37, no. 9, pp. 2484–2491, 1988.

[28] S. K. Das, J. E. Alam, and P. Mohanty, "Drag of heavy quarks in quark gluon plasma at energies available at the CERN Large Hadron Collider (LHC)," *Physical Review C*, vol. 82, no. 1, Article ID 014908, 2010.

[29] G. D. Moore and D. Teaney, "How much do heavy quarks thermalize in a heavy ion collision?" *Physical Review C*, vol. 71, no. 6, Article ID 064904, 19 pages, 2005.

[30] S. K. Das, J.-E. Alam, and P. Mohanty, "Probing quark gluon plasma properties by heavy flavors," *Physical Review C—Nuclear Physics*, vol. 80, no. 5, Article ID 054916, 2009.

[31] E. Schnedermann, J. Sollfrank, and U. Heinz, "Thermal phenomenology of hadrons from 200-A GeV S + S collisions," *Physical Review C*, vol. 48, no. 5, pp. 2462–2475, 1993.